Published in final edited form as:
Cancer Cell. 2012 April 17; 21(4): 532–546. doi:10.1016/j.ccr.2012.02.019.

VHL-regulated miR-204 Suppresses Tumor Growth through Inhibition of LC3B-mediated Autophagy in Renal Clear Cell Carcinoma

Olga Mikhaylova[1,6], **Yiwen Stratton**[1,6], **Daniel Hall**[1], **Emily Kellner**[1], **Birgit Ehmer**[1], **Angela F. Drew**[1], **Catherine A. Gallo**[1], **David R. Plas**[1], **Jacek Biesiada**[3], **Jarek Meller**[2,3], and **Maria F. Czyzyk-Krzeska**[1,4,5]

[1]Department of Cancer and Cell Biology, University of Cincinnati College of Medicine, Cincinnati, OH, 45267-0505

[2]Department of Environmental Health, University of Cincinnati College of Medicine, Cincinnati, OH 45267-0056

[3]Division of Biomedical Informatics Cincinnati Children's Hospital Medical Center, Cincinnati, OH 45229

[4]VA Research Service, Department of Veterans Affairs, Cincinnati, OH 45220

Summary

The von Hippel-Lindau tumor-suppressor gene (*VHL*) is lost in most clear cell renal cell carcinomas (ccRCC). Here, using human ccRCC specimens, VHL-deficient cells, and xenograft models, we show that miR-204 is a VHL-regulated tumor suppressor acting by inhibiting macroautophagy, with MAP1LC3B (LC3B) as a direct and functional target. Importantly, higher tumor grade of human ccRCC was correlated with a concomitant decrease in miR-204 and increase in LC3B levels, indicating that LC3B-mediated macroautophagy is necessary for RCC progression. VHL, in addition to inducing endogenous miR-204, triggered the expression of LC3C, an HIF-regulated LC3B paralog, that suppressed tumor growth. These data reveal a function of VHL as a tumor suppressing regulator of autophagic programs.

INTRODUCTION

Clear cell renal cell carcinoma (ccRCC), the most frequent and malignant type of renal cancer, is characterized by early loss of the von Hippel-Lindau tumor-suppressor gene (*VHL*) in a majority (60%–80%) of tumors. One well-recognized oncogenic effect of *VHL* loss is induction of the hypoxia inducible factor (HIF) and HIF-regulated genes, which stimulate angiogenesis and thus provide nutrients necessary for tumor growth (Gossage & Eisen, 2010). Discovery of this pathway laid the groundwork for the development of several anti-angiogenic therapeutic approaches for treatment of ccRCC (Heng & Bukowski, 2008). However, anti-angiogenic therapies have not lived up to their initial promise, which suggests

[5]Corresponding author: Maria F. Czyzyk-Krzeska, M.D., Ph.D., Department of Cancer and Cell Biology, The Vontz Center for Molecular Studies, University of Cincinnati College of Medicine, 3125 Eden Avenue, Cincinnati, OH 45267-0521, Tel: (513) 558-1957, Fax: (513) 558-5422, Maria.Czyzykkrzeska@uc.edu.
[6]The first two authors contributed equally to the manuscript.

that tumor growth and survival might be supported by alternative sources of nutrients such as autophagy.

Autophagy is a complex and tightly regulated homeostatic process that allows a cell to eliminate defective organelles and molecules and to recycle nutrients for survival under deprived conditions. Dependence of cancer cells on such oncogenic autophagy has been demonstrated (Degenhardt et al., 2006, Jin et al., 2007). Conversely, changes in the rate of autophagy may result in metabolic imbalance and cell death (Mathew et al., 2007, White & DiPaola, 2009). Classic macroautophagy involves a process utilizing ubiquitin-like cascades of ATG proteins leading to the formation of double-membrane autophagosomes containing cytoplasm, ribosomes, and other organelles. Autophagosomes ultimately fuse with lysosomes and targeting the cargo for proteolytic degradation (He & Klionsky, 2009). The initial step includes formation of an isolation membrane (phagophore), which can originate from the endoplasmic reticulum (Axe et al., 2008), outer mitochondrial membrane (Hailey et al., 2010), or plasma membrane (Ravikumar et al., 2010). The diverse origins of membranes for autophagic vacuoles create the possibility for adaptive and alternative autophagic programs that can be activated during different types or durations of starvation in a cell-type-specific manner. Phagophores interact with several regulatory multiprotein complexes, including mTOR and AMPK-regulated ULK complexes and the Beclin 1/class III PI3K complex. Further processing of the phagophore to the mature autophagosome requires covalent conjugation of ATG12 to ATG5 via a mechanism involving the E1-like enzyme ATG7 and the E2-like enzyme ATG10. The ATG12-ATG5 conjugate forms a complex with ATG16L and carries the final E3-like conjugation of the microtubule-associated protein light chain (MAP1LC3, here referred to as LC3) on an exposed C-terminal glycine to phosphatidylethanolamine (PE) initiated by the ubiquitinylation-like cascade processed by ATG7(E1) and ATG3 (E2) factors (Tanida et al., 2004). The appearance of the lipidated form of LC3 (LC3-II) in the autophagosome membrane is a commonly used marker of ongoing autophagy, and can be quantified by end-point flux analysis in the presence of lysosomal inhibitors (Rubinsztein et al., 2009, Klionsky et al., 2008).

In contrast to a single LC3 (ATG8) in yeast, mammalian cells have six different orthologs of ATG8 (LC3A, LC3B, LC3C, GABARAP, GABARAPL1, and GATE16/GABARAPL2) (Tanida et al., 2004). While tissue-specific patterns of expression and intracellular localization have been reported (Tanida et al., 2004), the precise functions of the individual orthologs are not well understood. Specific involvement of the different orthologs at different stages of autophagosome formation was observed in HeLa cells, with the LC3 family participating in earlier stages of autophagosome membrane elongation, and the GABARAP family involved in later stages of maturation (Weidberg et al., 2010). At least some functional redundancy among orthologs is expected based on similarities in sequence and structure (Wu et al., 2006) and the overlapping partner-protein binding patterns (Behrends et al., 2010). Interestingly, an alternative ATG5-/ATG7-/LC3B-independent pathway of autophagy has been described, wherein autophagosomes are derived from trans-Golgi and late endosomes in a RAB9-dependent manner (Nishida et al., 2009). The existence of multiple autophagic programs suggests differential functions dependent on the cellular context. Therapeutic manipulations of autophagy may provide anti-cancer treatments alternative to or supporting of anti-angiogenic therapies. In that respect, the small-molecule STF-62247 has been identified as a stimulator of autophagy leading to cell death and inhibition of RCC growth in xenograft models (Turcotte et al., 2008). On the other hand, inhibition of autophagy by chloroquine appears to cause robust tumor regression in the case of pancreatic cancer (Yang et al., 2011). Thus, autophagy represents a therapeutic target in need of further investigation.

MicroRNAs (miRs) are small noncoding RNAs that modulate gene expression (Selbach et al., 2008). There is ample evidence that miRs have regulatory functions in cancer initiation, progression, and metastasis (Lu et al., 2005, Calin & Croce, 2006). Introduction of stabilized miRs may restore lost tumor-suppressor activity (Czech, 2006, Negrini et al., 2007, Tong et al., 2008, Kota et al., 2009). Conversely, the use of antagomirs may allow for a decrease in the level and activity of miRs that promote oncogenesis (Krutzfeldt et al., 2005). MiR-204 is expressed from the large intron 6 of *TRPM3*, which is located on chromosome 9q21.12 and encodes a transient receptor potential, Ca^{2+}-permeable, non-selective cation channel (Oberwinkler & Phillipp, 2007) (Figure 1A). Both miR-204 and TRPM3 are expressed at higher levels in human kidney as compared with other organ tested (Lu et al., 2005).

Here, we investigate the role of VHL and miR-204 in the regulation of autophagic programs in ccRCC.

RESULTS

MiR-204 acts as a tumor suppressor in RCC

We analyzed the expression of miR-204 in 128 human ccRCC with known *VHL* status and, in 114 cases, a matched normal kidney specimen. The miR-204 level was significantly decreased in ccRCC as compared with matched normal kidney tissue in both paired (Figure 1B) and unpaired (not shown) analyses. MiR-211(Figure S1A), is a miR-204 paralog expressed from intron 6 of *TRPM1* on chromosome 15q13.3. Steady-state levels of miR-211 were also reduced in tumors as compared to normal kidneys, but the absolute expression levels of this miR were about 100-fold lower than that of miR-204 (Figure 1B). In contrast, HIF-inducible miR-210 (Kulshreshatha et al., 2007) was uniformly induced in ccRCC as compared with normal kidney, as reported by others (Figure. 1B) (Nakada et al., 2008, Jung et al., 2009, Juan et al., 2010).

MiR-204 inhibited the growth of RCC in two different xenograft models. In the first model, intratumoral injections of lentivirus particles containing wild-type pre-miR-204 arrested subcutaneous tumor growth, as compared with tumors injected with the same titer (10^7) of miR-204 carrying a 3-nucleotide mutation of its seed sequence (Figures 1C and S1A) which does not have miR-204 activity (see Figure 3Bb). The levels of wild-type miR-204 were in the range of miR-204 levels in normal kidneys (Figure S1B). Inhibition of tumor growth was accompanied by areas of focal necrosis, which stained positively for the necrosis marker C9, in the tumor regions directly exposed to injections (Figure 1D). Such necrosis was not observed in tumors injected with mutated miR-204 (Figure 1D). In an independent series of experiments, 786-O VHL(−) cells were transduced with lentiviral particles containing wild-type or mutated pre-miR-204 then injected under the kidney capsules of nude mice. In each case, initial transduction efficiency was determined to be above 95% based on the number of cells expressing GFP (Figure S1C), and the expression levels of miR-204 were also in the range of that measured in normal kidneys (Figure S1B). While the effect of miR-204 expression on tumor incidence was relatively small, there was a large decrease in the growth of tumors upon expression of miR-204 (Figure 1Ea). Moreover, tumors formed by 786-O cells expressing miR-204 were confined to the injection site under the capsule, with no infiltration of the kidney parenchyma (Figures 1Eb and 1Ec). In contrast, cells transduced with inactive mutant miR-204 formed highly invasive tumors that extensively infiltrated the kidney (Figures 1Ed). Taken together, these results indicate that miR-204 has tumor-suppressing activity.

MiR-204 is regulated by VHL

Consistent with the RCC tumor data, miR-204 levels in VHL(−) 786-O and A498 RCC cells were very low. Expression of miR-204, but not miR-211, was induced by reconstitution of

wild-type VHL in 786-O and A498 cells, while expression of miR-210 was repressed under the same conditions, as expected (Figure 2A). Conversely, VHL knockdown in the VHL-positive Caki-1 cell line led to decreased expression of miR-204 (Figure 2B). Moreover, there was a positive and significant correlation between normalized miR-204 levels and VHL protein levels in normal human kidneys (Figures 2C and 2D). We also found that VHL-induced expression of miR-204 correlated with expression of two short transcripts from *TRPM3*, TRPM3-005 and -010, but not with expression of the large transcript encoding the full-length protein (Figures S2A and S2B). A transcriptional module with a putative promoter was identified upstream from the first exon of these short transcripts, suggesting that miR-204 is co-expressed with transcripts that do not encode the full-length protein. We have also determined that expression of miR-204 was not regulated by hypoxia lasting from 8 to 48 hr (Figure S2C), treatment with prolyl hydroxylase inhibitor, DMOG, (Figure S2D), or inhibition of HIF-2α by siRNAs (Figure S2E), while all these treatments altered expression of HIF-regulated miR-210 as predicted. These data establish that VHL positively regulates expression of miR-204 in a manner most likely coordinate with some of the TRPM3 transcripts but independent of HIF activity.

MiR-204 is cytotoxic to VHL(−) but not VHL(+) cells

In our search for the tumor-suppressing mechanism of miR-204, we found that expression of exogenous miR-204 in VHL(−) cells was cytotoxic if cells were cultured in starvation conditions (Figures 3A and 3B). Importantly, the same dose of exogenous miR-204 was not cytotoxic to 786-O or A498 RCC cells reconstituted with wild-type VHL, which show several features of normal epithelial cells and are characterized by suppressed ability to form tumors in xenograft models, or to HK-2-immortalized renal epithelial cells (Figure 3Ba). The levels of exogenous miR-204 measured in VHL(−) or VHL(+) RCC cells or HK2 cells a were very similar. The effect required miR-204 targeting activity as mutation of three nucleotides within the core binding site of miR-204 abolished this cytotoxic effect (Figure 3Bb). Figure 3C shows an example of dying VHL(−) cells with extensive cytoplasmic vacuolization, in contrast to healthy VHL(+) cells. The cytotoxic effect of miR-204 was significantly attenuated when cells were continuously grown in 10% serum (Figure 3Bb). Similarly, if VHL(−) RCC cells starved for 48 hr were treated with fresh medium containing 10% FCS for 6 hr before miR-204 was applied, the cytotoxic effect of miR-204 was greatly diminished (Figure 3D). Moreover, when cells were treated with 10 mM glucose 16 hr after addition of miR-204 (before the beginning of massive cell death), cell death was greatly reduced (Figure 3E), suggesting that cell death resulted from starvation.

By using different approaches, we excluded a role for caspase-mediated apoptosis (Figures S3A and S3B), necroptosis (Figure S3C), or cathepsin-mediated cell death as causes of the cell death (Figures S3D). Moreover, at the cell densities used in these experiments, all VHL(−) and VHL(+) cells proliferated at similar rates and no differences in their cell cycle kinetics were observed, despite starvation (not shown).

MiR-204 inhibits macroautophagy downstream of autophagosome initiation

The above findings prompted us to investigate the role of miR-204 in the regulation of starvation-induced autophagy. Treatment with miR-204 did not cause additional cell death after autophagy was inhibited with an upstream inhibitor of macroautophagy, 3-methyladenine (Figure S4A). Moreover, similar to the effects of miR-204, inhibition of autophagy by knockdown of the upstream regulator, ATG5, resulted in significantly higher death of VHL(−) cells as compared to VHL(+) cells (Figure S4B), supporting the idea that VHL(−) cells are more dependent on autophagy and therefore more sensitive to its inhibition.

Using transmission electron microscopy (TEM) to quantify the number of autophagic vesicles, we found that treatment with miR-204 significantly reduced the number of autophagic vesicles in VHL(−) but not in VHL(+) cells, an effect measured in both the presence and absence of the autophagy inhibitor, chloroquine (Figure 4A). Moreover the vesicles present in VHL(−) cells treated with miR-204 were smaller and less developed as compared with those in the untreated cells. This indicates that miR-204 inhibits the formation of autophagic vesicles.

Next we determined whether miR-204 exerted its effect during autophagosome initiation or maturation. MiR-204 did not alter mTORC1 pathway activity (Figure S4C), indicating that the effects of miR-204 were not mediated by inhibition of this pathway. Recently, Weidberg et al., (2010) reported that inhibition of autophagy by knocking down subfamilies of LC3s or GABARAPs, which function at the level of autophagosome maturation, resulted in the accumulation of upstream regulators that participate in forming the initial membranes, such as ATG12-ATG5 and ATG16L punctate structures. Treatment with miR-204 alone significantly increased the number of cells expressing both ATG5-ATG12 and ATG16L punctate structures and induced an increase in the number of ATG16L puncta per cell in VHL(−) cells, but not in VHL(+) cells, grown in 0.1% serum (Figures 4B, 4C, S4D). Inhibition of autophagy by chloroquine alone also resulted in increased numbers of VHL(−) 786-O and A498 cells expressing ATG5-ATG12 puncta, with the effects significantly weaker in VHL(+) cells (Figure 4B). Chloroquine alone had a stronger effect in VHL(−) cells than miR-204 alone, and simultaneous treatment with both agents resulted in an accumulation of a similar magnitude to that induced by chloroquine alone. In the case of ATG16L puncta, chloroquine and miR-204 had similar effects on the number of cells with these puncta, particularly in 786-O cells (Figures 4C and S4D). Taken together, these data suggest that miR-204 exerts its effect downstream of the formation of the initial phagophore membranes and possibly at the level of autophagosome maturation.

The presence of the lipidated form of LC3 (LC3-II) in the autophagosome membrane is a marker of effective autophagy, we therefore measured accumulation of the lipidated forms of the LC3s and GABARAPs. The accumulation of LC3B-II was inhibited in VHL(−) cells by miR-204 in the absence of chloroquine (Figure 5A, lanes 6 and 5 in each panel). Treatment with chloroquine, as expected, induced accumulation of LC3B-II (Figure 5A, compare lanes 7 vs. 5), but miR-204 inhibited this accumulation by two to three fold as well (Figure 5A, compare lanes 7 and 8). In contrast, while LC3B-II accumulated in response to chloroquine in VHL(+) cells, this response was not affected by miR-204 (Figure 5A lanes 1–4). Similarly, while increased accumulation of LC3B-II was observed in HK-2 cells in response to chloroquine, levels of LC3B-II were not affected by miR-204 (Figure S5A). Treatment with miR-204 had no effect on the expression of LC3B mRNA in either cell line (Figure S5B). The accumulation of LC3A-II was not affected by VHL or miR-204 in any consistent manner. Surprisingly, LC3C-II was expressed only in VHL(+) RCC cells. Among the GABARAP-like proteins, only GABARAPL2-II showed slightly decreased expression in response to miR-204 (Figure 5A), and the dependence of its overall expression on VHL varied depending on the cell line. GABARP-II was predominantly expressed in 786-O VHL(+) cells and barely detectable in A498 cells. We were unable to detect expression of GABARAPL1 protein. Immunofluorescence staining confirmed the effects of miR-204 on the endogenous LC3B in VHL(−) and VHL(+) RCC cells (Figure S5C) and the results were consistent with the accumulation of LC3B-II as measured by western blot (Figure 5A). Overall, these data indicate that miR-204 inhibits starvation-induced macroautophagy in VHL(−) but not VHL(+) RCC cells at the stages of autophagosome maturation, and not at initiation.

Knockdown of LC3B resulted in a significantly higher rate of cell death in VHL(−) cells as compared with VHL(+) cells in both 786-O and A498 cells (Figures 5B, S5D). This result further supports the concept of a specific dependence of VHL(−) cells on an ATG5/LC3B/miR-204–regulated autophagic program.

LC3B is a direct target of miR-204 and it is necessary for miR-204 cytotoxic activity

To identify specific miR-204 targets with potential relevance in the regulation of autophagy, we used several miR target-prediction algorithms (Pictar, TargetScan, Miranda, Sanger) and found conserved miR-204 sites in the 3'UTRs of two direct regulators of autophagy, LC3B and LC3B2. Because LC3B2 is not expressed in 786-O cells, we concentrated our further analysis on LC3B.

The miR-204 binding site in LC3B mRNA is a broadly conserved element located between 55 and 61 bp of the LC3B 3'UTR (Figure 6Aa). The 3'UTR of LC3B with the wild-type, but not with a mutant, miR-204–binding site conferred repression by miR-204 to a luciferase reporter (Figure 6Ab). Furthermore, as expected, inhibition of miR-204 activity by using miRZip anti-204 (Mavrakis et al. 2010, Veronese et al., 2010, Loven et al., 2010) or siRNA (80%–90% knockdown) upregulated LC3B protein expression in VHL(+) RCC cells (Figure 6B), indicating that LC3B is under constitutive repression by endogenous miR-204. This observation was further supported by a significant negative correlation between levels of miR-204 and LC3B protein in the subpopulation of human ccRCC tumors with the wild-type *VHL* (Figures 6C and 6D). Importantly, the increased accumulation of LC3B-II in the presence of chloroquine in VHL(+) 786-O cells with miR-204 knocked down, as compared with control VHL(+) cells, indicates an induction of macroautophagy (Figure 6E, lanes 3 and 4). Moreover, levels of endogenous LC3B were higher in VHL(−) as compared with VHL(+) RCC cells (Figure 5A), consistent with higher levels of endogenous miR-204 in VHL(+) cells.

Most importantly, re-expression of LC3B lacking the 3'UTR, and therefore insensitive to miR-204, protected VHL(−) 786-O cells from miR-204 cytotoxicity (Figure 6F). Cells from the same transfection that had lost LC3B-RFP (RFP-negative cells) or cells transfected with RFP alone demonstrated significant miR-204–induced cytotoxicity (Figure 6F). This rescue from cell death by expression of RFP-LC3B was accompanied by a reduction in the accumulation of ATG16L-positive puncta in response to miR-204 in RFP-LC3B–transfected cells (Figures 6G and S6A-S6B) as compared to the effect of miR-204 on nontransfected cells (RFP-negative cells) or cells transfected with RFP alone (Figure 6G and Figures S6C-S6D).

Next we asked if miR-204 was cytotoxic to cells with LC3B knocked down. In the first approach, we used 786-O and A498 pools of cells with LC3B stably knocked down (Figure S6E). Because all cells with stable LC3B knockdown grew very slowly and progressively died in medium containing 0.1% serum, they were initially seeded in higher numbers to assure a similar degree of confluence for cells in the control and LC3B knockdown pools at the time of treatment with miR-204. Under these conditions, miR-204 did not have a cytotoxic effect on 786-O or A498 cells with LC3B knockdown, but remained cytotoxic to the control cells (Figure 6H). We also performed another experiment where VHL(−) cells were plated at the same densities, starved as in Figure 3A, and then transiently transfected with miR-204, siRNA for LC3B, or both, along with the respective negative controls (Figure S6F). The effects of miR-204 and LC3B siRNA on cell death were similar, and there was no additional effect when miR-204 and LC3B siRNA were applied together (Figure S6F).

LC3C protects VHL(+) RCC cells from loss of LC3B-mediated autophagy

The presence of VHL protected RCC cells from the cytotoxic effects of miR-204 and LC3B knockdown. We found that VHL is a strong inducer of a largely uncharacterized LC3B paralog, LC3C (Figures 5A, 7A, S7A). Reconstitution of VHL in RCC cells induced (Figures 5A and 7A), while knockdown of VHL in Caki-1 cells (Figure S7A) reduced expression of LC3C-II. This regulation occurred at the level of mRNA (Figure 7B) and was responsive to HIF-2α. Knockdown of HIF-2α induced LC3C mRNA (Figure 7C), while activation of HIF-2α using DMOG repressed LC3C mRNA (Figure 7D). The high levels of LC3C in VHL(+) cells suggested that LC3C may protect VHL(+) cells from inhibition of LC3B-mediated autophagy. Testing this possibility, we found that single LC3C knockdown (Figure S7B) had comparable to the single knockdown of LC3B and relatively minor effect on VHL(+) cell survival in response to serum starvation, while double LC3B/LC3C knockdown (Figure S7B) reduced the viability of VHL(+) cells to the levels measured in VHL(−) cells (Figure 7E).

LC3B-dependent autophagy is necessary for RCC tumor growth

We then tested the hypothesis that LC3B-mediated autophagy is necessary for tumor growth. Injection of pre-formed subcutaneous tumors with lentiviral particles containing shRNAs against LC3B or ATG5 every other day for 9 days resulted in significant inhibition of tumor growth, as compared with tumors injected with scrambled shRNA (Figure 8A). A similar result was obtained when cell lines with stable expression of shRNA targeting LC3B or ATG5 were injected into the kidneys of nude mice, and growth of orthotopic tumors was determined after 10 weeks. 786-O VHL(-) cells formed tumors in 83% of mice, which was a reproducible incidence in at least 5 independent experimental series performed in our laboratory over the last two years (see also Yi et al., 2010). In contrast, injection of cells with knockdown of LC3B or ATG5 resulted in reduced tumor growth (Figure 8B). Similar results were obtained using A498 cells, where the formation of tumors was completely inhibited by the knockdown of either LC3B or ATG5 (Figure 8C). These data indicate that ATG5/LC3B-mediated macroautophagy is necessary for the growth of VHL(−) RCC tumors in nude mice.

Next, we determined the status of LC3B and ATG5 in 102 human kidney-ccRCC tumor pairs by using quantitative immunoblotting with a set of reference standards to normalize results from multiple blots (Yi et al., 2010). We found a significant correlation between tumor-kidney ratios of the normalized protein levels for LC3B (all three forms) and ATG5 (Figure S8A). Importantly, we found that LC3B levels positively correlated with tumor grade, while miR-204 levels showed a negative correlation (Figure 8D) suggesting that loss of miR-204 and activation of autophagy are critical regulators of cancer progression in sporadic human ccRCC.

Finally, we tested the role of LC3C in the tumor-suppressing activity of VHL. Knockdown of LC3C in VHL(+) 786-O and A498 cells (Figure S7B) increased the incidence of small tumor formation by both cell lines when injected into the kidneys of nude mice (Figure 8E). Moreover, analysis of the human ccRCC kidney-tumor pairs revealed decrease in LC3C protein expression in majority of tumors (Figure S8B). These results support the role of LC3C as a regulator of an autophagic program involved in tumor suppression.

DISCUSSION

A large majority of human ccRCC is characterized by early loss of *VHL*. Here, we identify two pathways that are regulated by VHL and contribute significantly, although in opposite direction, to ccRCC tumor growth (Figure 8F). The data clearly demonstrate that formation of RCC tumors by VHL(−) RCC cells in nude mice requires active LC3B/ATG5-dependent

autophagy. Consistent with this, progression of human ccRCC is associated with increasing levels of LC3B protein. We propose that the crucial event leading to activation of this pro-tumorigenic autophagic program is the loss of miR-204 and de-repression of LC3B, which in turn, stimulates and/or maintains autophagy. It is also likely that miR-204 regulates a network of targets that influence macroautophagy through mechanisms and pathways converging at the level of LC3B and maturation of the autophagosome, without affecting phagophore initiation. This renders cancer cells addicted to macroautophagic activity, and, thus, subject to synthetic lethality when macroautophagy is inhibited by exogenous miR-204, with necrotic cell death caused by starvation.

We have also discovered that VHL, through inhibition of HIF, induces LC3C. LC3C, so far uncharacterized, contributes to basic autophagic activity in VHL(+) cells at a level similar to LC3B, but it also mediates an anti-tumorigenic autophagic activity as its knockdown increased the incidence of small tumors in VHL(+) cells. At present, the biochemical activity of such a program is not understood, but there is growing evidence for autophagic programs that are not mediated by ATG5/LC3B (Nishida et al., 2009) or ULK1/2 (Cheong et al., 2011). Thus, LC3C could be a part of such yet unidentified pathway, or could participate in a non-autophagic tumor-suppressing pathway. Moreover, an LC3C-specific autophagic program could have selectivity towards specific pro-oncogenic targets. Interestingly, the potential functional differences between LC3C and LC3B/LC3A could be related to the fact that LC3C contains an unstructured C-terminus domain that is not present in other family members. The mechanism by which HIF represses expression of LC3C remains to be investigated, but the LC3C proximal promoter contains E2-boxes, similar to those that mediate HIF-dependent inhibition of E-cadherin mRNA by ZFHX1B and SNAI1 (Estaban et al., 2006, Evan et al., 2007).

The requirement for macroautophagy in RCC cells, and the protective activity of LC3C in normal cells, creates a unique opportunity for the use of miR-204 or miR-204–like approaches in the treatment of RCC. Such strategies would spare normal epithelial cells while killing malignant tumor cells. In particular, a therapeutic approach inducing cytotoxic, rather than cytostatic effects is desirable as the currently used anti-angiogenic treatments are only cytostatic. Importantly, treatments for pancreatic cancer involving general inhibitors of autophagy, such as chloroquine, are currently in clinical trials (Yang et al., 2011).

While VHL is a positive regulator of miR-204 expression in normal tissues, it is likely that factors additional to the loss of VHL could trigger decreased miR-204 expression, particularly during cancer progression. In that respect, miR-204 is expressed from locus 9q21.12, and published data indicate that chromosome 9 is the second most frequently lost chromosome, after 3p, in RCC (20%-30% of tumors) decreased expression of genes from this region (Fukunaga et al., 2002, Yoshimoto et al., 2007, Toma et al., 2008). Our initial evidence points towards coordinated expression of miR-204 with short, but not full-size, TRPM3 transcripts, which could represent a more general mechanism for expression of intronic miRs from long genes.

Taken together, our findings indicate that VHL regulates at least two autophagic programs, through an HIF-independent pathway activating miR-204 and an HIF-regulated pathway activating LC3C.

EXPERIMENTAL PROCEDURES

Human RCC tumors

Fresh-frozen samples of renal clear cell carcinomas (n=128) and matched normal kidneys (n=114) were obtained and analyzed for *VHL* gene sequence and protein expression as

described before (Yi et al., 2010). Specimens were also analyzed for expression of miR-204, miR-211, and miR-210. All human samples were anonymous and exempted from IRB protocol.

Cell culture methods and treatments

Pools of human VHL(−) and VHL(+) 786-O and Caki-1 cells were described by us before (Mikhaylova et a., 2008, Yi et al., 2010); A498 cells were obtained from Dr. W. G. Kaelin Jr., (DFI, Harvard medical School). HK-2 cells were purchased from ATCC. All cells were authenticated (Genetica, Cincinnati, OH). For miR-204 treatments, cells were plated in 12-well cell culture dishes at 3,000 per well in normal medium. 24 hr later, the medium was replaced with fresh medium containing 10% or 0.1% serum. After the next 48 hr, cells were transduced with lentiviral particles containing wild-type or mutated pri-miR-204, or transfected with the respective short pre-miR-204, in each case with the appropriate negative controls. Cell viability was determined 48 hr after miR-204 treatment by trypan blue exclusion. For the LC3-II flux experiments, cells were plated and treated as described above, and 24 hr after miR-204 treatment, cells were treated with 100 μM chloroquine to inhibit lysosomal function. Cells were collected at the indicated times and analyzed by PAGE for the proteins of interest.

Quantitative RT-PCR

Total RNA was extracted using the mirVana miRNA Isolation kit (Ambion). For microRNA analysis, the samples were first reverse transcribed using the TaqMan microRNA Reverse Transcription kit and miR-specific primers and probes (TaqMan microRNA Assays, Applied Biosystems), and quantified with real-time PCR on an Applied Biosystems 7900HT Fast Real-Time PCR System. The small nucleolar RNA (snoRNA) RNU44 was used as the internal control for the $-\Delta Ct$ calculation. Data are presented normalized to snoRNU44, or as ratios of the normalized values between paired cell lines differing in the status of VHL or tumor/kidney pairs. For mRNA, qRT-PCR was performed as described before (Yi et al., 2010) and the sequence of primers is provided in the Supplemental Experimental Procedures.

Constructs and plasmids

The following miR-204 reagents were used: Pre-miR-204 precursor and Pre-miR negative control were purchased from Ambion (Pre-miR-204™ miRNA Precursor Molecules, and negative control Pre-miR™ miRNA Precursor Molecule). Anti-miR-204 and the corresponding negative control were purchased from Dharmacon (miRIDIAN Hairpin Inhibitor: human hsa-miR-204, and miRIDIAN microRNA Hairpin Inhibitor Negative Control #1). HIV-based lenti-miR pri-micro RNA-204 construct and control lentivector were from System Biosciences (microRNA Expression Construct Lenti-miR-204 MI0000284 and corresponding lentivector negative control). To alter the miR-204 core sequence, site-directed mutagenesis was performed on PMIRH204 to replace the core CCC sequence with a GGG sequence (GenScript). The mutation was verified by sequencing. List of siRNA and shRNA constructs is provided in the Supplemental Experimental Procedures. All lentiviral DNA constructs were VSV-G envelope packaged (Cincinnati Children's Hospital Medical Center Viral Vector Core) and infected into cells followed by plasmid-appropriate selection. The LC3B-RFP construct contained human LC3B-myc fused to RFP from pDsRed1-N1 in the PRK5 vector and was a gift from Drs. P. Dennis and C. Mercer (University of Cincinnati). The Luciferase-LC3B-3'UTR construct was based on pLightSwitch_3'UTR vector and purchased from Switchgear Genomics.

Transfections and transduction experiments

Transient transfections of microRNA constructs or pools of siRNAs were performed using Lipofectamine 2000 according to the manufacturer's protocol. Transductions with lentiviral particles were performed using 2 μg/ml of polybrene.

Western blot analysis

Total cellular lysates were obtained by lysing cells in RIPA buffer containing proteinase and phosphatase inhibitors. 5 to 30 μg of extracts were separated on 12% polyacrylamide gels and transferred onto PVDF membrane. Blots were probed with relevant antibodies described in Supplemental Experimental Procedures. Quantitative immunoblotting for human RCC tumors and matched kidneys was performed as described in (Yi et al., 2010).

Mouse xenograft experiments

All experiments on mice were performed in accordance with University of Cincinnati IACUC approved protocol. For the intra-kidney injections, 30,000 cells were resuspended in Matrigel to a final volume of 30 μl, and then slowly injected into the parenchyma of the kidneys of 4- to 5-week-old athymic nude mice and tumors were collected after 10–12 weeks. For the subcutaneous injections, 1x 10^6 cells in cell culture medium were injected subcutaneously into the flanks of the same strain of nude mice. After 6 weeks, these tumors reached an approximate average volume of 50 mm^3 and mice were randomly assigned to groups in which the tumors would be injected with specific viral particles containing constructs encoding mutant miR-204, wild-type miR-204, or specific shRNAs. For each control and experimental condition, the same titer of viral particles was used. Injections were performed with 25 μl of supernatant every other day for a period of 9 days. Before injections, three standard dimensions of the tumor were measured with a protractor and the volume of the tumor was calculated using the equation $d1 \times d2 \times d3 \times \pi/6$. At the end of the experiments, mice were sacrificed and tumors were fixed in 4% paraformaldehyde, paraffin embedded, and H&E stained or processed for immunocytochemistry using a monoclonal antibody against Complement Component 9 (Vector Laboratories).

Immunofluorescence staining

Cells were plated on coverslips and treated with miR-204. At the end of the experiment, cells were fixed in 4% paraformaldehyde, permeabilized, and blocked in 0.3% Triton and 0.1% Triton with 3% BSA, and incubated with primary antibody for 1hr at 37°C. Cells were then washed and incubated with the Alexa 488-labeled secondary antibody for 1h at room temperature. Confocal images were acquired on a Zeiss LSM510 confocal or by using a Zeiss Axioplan 2 microscope with the appropriate filter cubes and a Zeiss Axiocam MRm to record the images. The number of cells expressing puncta and the number of puncta per cell were counted manually.

Preparation of samples and TEM

Samples were processed in the Electron Microscopy Core at Cincinnati Children's Hospital Medical Center. Briefly, cells were washed with PBS and resuspended in 0.2 M cacodylate buffer with 3% glutaraldehyde. Cells were post-fixed with 1% Osmium tetroxide (Electron Microscopy Sciences, Fort Washington, PA) with 0.2 M sodium cacodylate buffer for 1 hour at 4°C. After three washes with 0.2 M sodium cacodylate buffer, cells were resuspended in 1% agarose (type IX, Sigma), centrifuged for 5 min at 3,000 rpm, and left for 24 hr at 4°C. The following day, samples were dehydrated and embedded in LX-112 embedding medium (Ladd Research Industries, Burlington, VT). Samples were then polymerized for 48 hr at 60°C, cut into 100 nm thick sections on a USA Reichert-Jung UltraCut E microtome, positioned on 200 mesh grids, and stained with uranyl acetate and

lead citrate. TEM was performed on a JEOL 1230 TEM at an accelerating voltage of 80kV. Images were acquired with an AMT Advantage Plus 2K x 2K digital camera connected to the TEM.

LC3B rescue experiments

Cells were plated at 85,000 cells per 60 mm plate in regular medium containing 10% FBS. Transfections with LC3B-RFP or RFP construct were performed 24 hr later using Lipofectamine LTX and PLUS reagent (Invitrogen) according to the manufacturer's protocol. Expression of RFP was clearly visible by 24 hr to 30 hr after transfection. Cells were then collected and sorted using a BD FACSAria. Sorted cells were plated at a density of 5,000 per well in 12-well plates in normal medium with 10% FBS with added antibiotics and antimycotics. 24 hr after plating, the medium was replaced with medium containing 0.1% serum. After 48 hr of starvation, cells were transfected with 25 nM of pre-miR-204 precursor or a negative control construct (Ambion) by using Lipofectamine 2000. On the last day, cells were collected, stained with DAPI to distinguish live cells, and the percentage of RFP+ cells was determined, among both viable and dead cell populations, by flow cytometry.

Statistical analysis

For descriptive statistics, data are expressed as mean ±SEM unless indicated otherwise. Analysis of differential expression was performed using one-way analysis of variance (ANOVA), followed by Tukey-Kramer multiple comparison tests. Differences where $P<0.05$ were considered to be statistically significant. In quantitative immunoblotting experiments, we used $\log_2$-transformed normalized values to facilitate robust and outlier-insensitive analyses. Standard box-and-whisker plots were used to compare distributions of the normalized abundance measure for individual proteins. Correlations between variables were assessed by means of regression analysis and by Pearson and Spearman rank correlation coefficients.

Supplementary Material

Refer to Web version on PubMed Central for supplementary material.

Acknowledgments

This work was supported in part by the following grants NCI CA122346, DoD W81XWH-07-02-0026, BLR&D VA Merit Award to MCK, and UC P30-ES006096 CEG; DRP and CAG were supported by NCI CA133164. We thank Drs. P. Dennis and C. Mercer for LC3B-RFP constructs, K. Winstead for the collection of human ccRCC tumors, Z. Shan for the histological preparation of tumor sections, G. Ciraolo for processing tissues for TEM, J. Neumann for injection of mice, G. Doerman for preparing the figures, Dr. M. Daston for editorial assistance, and undergraduate students P. Bastola and P.J. Krzeski for technical assistance.

References

Axe EL, Walker SA, Manifava M, Chandra P, Roderick HL, Habermann A, Griffiths G, Ktistakis NT. Autophagosome formation from membrane compartments enriched in phosphatidylinositol 3-phosphate and dynamically connected to the endoplasmic reticulum. J Cell Biol. 2008; 18:685–701. [PubMed: 18725538]

Behrends C, Sowa ME, Gygi SP, Harper JW. Network organization of the human autophagy system. Nature. 2010; 466:68–76. [PubMed: 20562859]

Calin GA, Croce CM. MicroRNA signatures in human cancers. Nat Rev Cancer. 2006; 6:857–866. [PubMed: 17060945]

Cheong H, Lindsten T, Wu J, Lu C, Thompson CB. Ammonia-induced autophagy is independent of ULK1/ULK2 kinases. Proc Natl Acad Sci USA. 2011; 108:11121–11126. [PubMed: 21690395]

Czech MP. MicroRNAs as therapeutic targets. N Engl J Med. 2006; 354:1194–1215. [PubMed: 16540623]

Degenhardt K, Mathew R, Beaudoin B, Bray K, Anderson D, Chen G, Mukherjee C, Shi Y, Gélinas C, Fan Y, Nelson DA, Jin S, White E. Autophagy promotes tumor cell survival and restricts necrosis, inflammation, and tumorigenesis. Cancer Cell. 2006; 10:51–64. [PubMed: 16843265]

Esteban MA, Tran MG, Harten SK, Hill P, Castellanos MC, Chandra A, Raval R, O'Brien TS, Maxwell PH. Regulation of E-cadherin expression by VHL and hypoxia-inducible factor. Cancer Res. 2006; 66:3567–3575. [PubMed: 16585181]

Evans AJ, Russell RC, Roche O, Burry TN, Fish JE, Chow VW, Kim WY, Saravanan A, Maynard MA, Gervais ML, et al. VHL promotes E2 box-dependent E-cadherin transcription by HIF-mediated regulation of SIP1 and snail. Mol Cell Biol. 2007; 27:157–169. [PubMed: 17060462]

Fukunaga K, Wada T, Matsumoto H, Yoshihiro S, Matsuyama H, Naito K. Renal cell carcinoma: allelic loss at chromosome 9 using the fluorescent multiplex-polymerase chain reaction technique. Hum Pathol. 2002; 33:910–914. [PubMed: 12378516]

Gossage L, Eisen T. Alterations in VHL as potential biomarkers in renal-cell carcinoma. Nat Rev Clin Oncol. 2010; 7:277–288. [PubMed: 20368728]

Hailey DW, Rambold AS, Satpute-Krishnan P, Mitra K, Sougrat R, Kim PK, Lippincott-Schwartz J. Mitochondria supply membranes for autophagosome biogenesis during starvation. Cell. 2010; 141:656–667. [PubMed: 20478256]

He C, Klionsky DJ. Regulation mechanisms and signaling pathways of autophagy. Ann Rev Genet. 2009; 43:67–93. [PubMed: 19653858]

Heng DY, Bukowski RM. Anti-angiogenic targets in the treatment of advanced renal cell carcinoma. Curr Cancer Drug Targets. 2008; 8:676–682. [PubMed: 19075590]

Jin S, DiPaola RS, Mathew R, White E. Metabolic catastrophe as a means to cancer cell death. J Cell Sci. 2007; 120:379–383. [PubMed: 17251378]

Juan D, Alexe G, Antes T, Liu H, Madabhushi A, Delisi C, Ganesan S, Bhanot G, Liou LS. Identification of a microRNA panel for clear-cell kidney cancer. Urology. 2010; 75:835–841. [PubMed: 20035975]

Jung M, Mollenkopf HJ, Grimm C, Wagner I, Albrecht M, Waller T, Pilarsky C, Johannsen M, Stephan C, Lehrach H, et al. MicroRNA profiling of clear cell renal cell cancer identifies a robust signature to define renal malignancy. J Cell Mol Med. 2009; 13:3918–3928. [PubMed: 19228262]

Klionsky DJ, Abeliovich H, Agostinis P, Agrawal DK, Aliev G, Askew DS, Baba M, Baehrecke EH, Bahr BA, Ballabio A, et al. Guidelines for the use and interpretation of assays for monitoring autophagy in higher eukaryotes. Autophagy. 2008; 4:151–175. [PubMed: 18188003]

Kota J, Chivukula RR, O'Donnell KA, Wentzel EA, Montgomery CL, Hwang HW, Chang TC, Vivekanandan P, Torbenson M, Clark KR, et al. Therapeutic microRNA delivery suppresses tumorigenesis in a murine liver cancer model. Cell. 2009; 137:1005–1017. [PubMed: 19524505]

Krützfeldt J, Rajewsky N, Braich R, Rajeev KG, Tuschl T, Manoharan M, Stoffel M. Silencing of microRNAs in vivo with 'antagomirs'. Nature. 2005; 438:685–689. [PubMed: 16258535]

Kulshreshtha R, Ferracin M, Wojcik SE, Garzon R, Alder H, Agosto-Perez FJ, Davuluri R, Liu CG, Croce CM, et al. A microRNA signature of hypoxia. Mol Cell Biol. 2007; 27:1859–1867. [PubMed: 17194750]

Lovén J, Zinin N, Wahlström T, Müller I, Brodin P, Fredlund E, Ribacke U, Pivarcsi A, Påhlman S, Henriksson M. MYCN-regulated microRNAs repress estrogen receptor-alpha (ESR1) expression and neuronal differentiation in human neuroblastoma. Proc Natl Acad Sci USA. 2010; 107:1553–1558. [PubMed: 20080637]

Lu J, Getz G, Miska EA, Alvarez-Saavedra E, Lamb J, Peck D, Sweet-Cordero A, Ebert BL, Mak RH, Ferrando, et al. MicroRNA expression profiles classify human cancers. Nature. 2005; 435:834–838. [PubMed: 15944708]

Mathew R, Karantza-Wadsworth V, White E. Role of autophagy in cancer. Nat Rev Cancer. 2007; 7:961–967. [PubMed: 17972889]

Mavrakis KJ, Wolfe AL, Oricchio E, Palomero T, de Keersmaecker K, McJunkin K, Zuber J, James T, Khan AA, Leslie CS, et al. Genome-wide RNA-mediated interference screen identifies miR-19

targets in Notch-induced T-cell acute lymphoblastic leukaemia. Nature Cell Biol. 2010; 12:372–379. [PubMed: 20190740]

Mikhaylova O, Ignacak ML, Barankiewicz TJ, Harbaugh SV, Yi Y, Maxwell PH, Schneider M, Van Geyte K, Carmeliet P, Revelo MP, et al. The von Hippel-Lindau tumor suppressor protein and Egl 9-type proline hydroxylases regulate the large subunit of RNA Polymerase II in response to oxidative stress. Mol Cell Biol. 2008; 28:2701–2717. [PubMed: 18285459]

Nakada C, Matsuura K, Tsukamoto Y, Tanigawa M, Yoshimoto T, Narimatsu T, Nguyen LT, Hijiya N, Uchida T, Sato F, et al. Genome-wide microRNA expression profiling in renal cell carcinoma: significant down-regulation of miR-141 and miR-200c. J Pathol. 2008; 216:418–427. [PubMed: 18925646]

Negrini M, Ferracin M, Sabbioni S, Croce CM. MicroRNAs in human cancer: from research to therapy. J Cell Sci. 2007; 120:1833–1840. [PubMed: 17515481]

Nishida Y, Arakawa S, Fujitani K, Yamaguchi H, Mizuta T, Kanaseki T, Komatsu M, Otsu K, Tsujimoto Y, Shimizu S. Discovery of Atg5/Atg7-independent alternative macroautophagy. Nature. 2009; 461:654–658. [PubMed: 19794493]

Oberwinkler J, Phillipp SE. TRPM3. Handb Exp Pharmacol. 2007; 179:253–67. [PubMed: 17217062]

Ravikumar B, Moreau K, Jahreiss L, Puri C, Rubinsztein DC. Plasma membrane contributes to the formation of pre-autophagosomal structures. Nat Cell Biol. 2010; 12:747–757. [PubMed: 20639872]

Rubinsztein DC, Cuervo AM, Ravikumar B, Sarkar S, Korolchuk V, Kaushik S, Klionsky DJ. In search of an "autophagomometer. " Autophagy. 2009; 5:585–589.

Selbach M, Schwanhäusser B, Thierfelder N, Fang Z, Khanin R, Rajewsky N. Widespread changes in protein synthesis induced by micro RNAs. Nature. 2008; 455:58–63. [PubMed: 18668040]

Tanida I, Ueno T, Kominami E. LC3 conjugation system in mammalian autophagy. Int J Biochem Cell Biol. 2004; 36:2503–2518. [PubMed: 15325588]

Toma MI, Grosser M, Herr A, Aust DE, Meye A, Hoefling C, Fuessel S, Wuttig D, Wirth MP, Baretton GB. Loss of heterozygosity and copy number abnormality in clear cell renal cell carcinoma discovered by high-density affymetrix 10K single nucleotide polymorphism mapping array. Neoplasia. 2008; 10:634–642. [PubMed: 18592004]

Tong AW, Nemunaitis J. Modulation of miRNA activity in human cancer: a new paradigm for cancer gene therapy? Cancer Gene Ther. 2008; 15:341–355. [PubMed: 18369380]

Turcotte S, Chan DA, Sutphin PD, Hay MP, Denny WA, Giaccia AJ. A molecule targeting VHL-deficient renal cell carcinoma that induces autophagy. Cancer Cell. 2008; 14:90–102. [PubMed: 18598947]

Veronese A, Lupini L, Consiglio J, Visone R, Ferracin M, Fornari F, Zanesi N, Alder H, D'Elia G, Gramantieri L, et al. Oncogenic Role of miR-483-3p at the IGF2/483 Locus. Cancer Res. 2010; 70:3140–3149. [PubMed: 20388800]

Weidberg H, Shvets E, Shpilka T, Shmiron F, Shinder V, Elazar Z. LC3 and GATE/GABARAP subfamilies are both essential yet act differently in autophagosome biogenesis. The EMBO J. 2010; 29:1792–1802.

White E, DiPaola RS. The double-edged sword of autophagy modulation in cancer. Clin Cancer Res. 2009; 15:5308–5316. [PubMed: 19706824]

Wu J, Dang Y, Su W, Liu C, Ma H, Shan Y, Pei Y, wan B, Guo J, Yo L. Molecular cloning and characterization of rat LC3A and LC3B- two novel markers of autophagosome. Biochem Biophys Res Comm. 2006; 339:437–442. [PubMed: 16300744]

Yi Y, Mikhaylova O, Mamedova A, Bastola P, Biesiada J, Alshaikh E, Levin L, Sheridan RM, Meller J, Czyzyk-Krzeska MF. VHL-dependent patterns of RNA Polymerase II hydroxylation in human renal clear cell carcinomas. Clin Cancer Res. 2010; 16:5142–5152. [PubMed: 20978146]

Yang S, Wang X, Contino G, Liesa M, Sahin E, Ying H, Bause A, Li Y, Stommel JN, Dell'Antonio G, et al. Pancreatic Cancers require autophagy for tumor growth. Genes & Dev. 2011; 25:717–729. [PubMed: 21406549]

Yoshimoto T, Matsuura K, Karnan S, Tagawa H, Nakada C, Tanigawa M, Tsukamoto Y, Uchida T, Kashima K, Akizuki S, et al. High-resolution analysis of DNA copy number alterations and gene expression in renal clear cell carcinoma. J Pathol. 2007; 213:392–401. [PubMed: 17922474]

Significance

ccRCC tumor growth depends on abundant angiogenesis and activation of glycolytic metabolic pathways that result from *VHL* loss and induction of hypoxia-inducible factor (HIF) and HIF targets. Here we show that loss of VHL also promotes, in an HIF-independent manner, access to nutrients from intracellular sources through activation of LC3B-mediated autophagy. This autophagic program is necessary for tumor growth. In addition, VHL, by repressing HIF, induces expression of LC3C, which exercises tumor-suppressing activity. These findings support a role for VHL as a tumor suppressor in the control of different autophagic programs. Addiction of cancer cells to oncogenic autophagy creates the possibility that miR-204 could be used in ccRCC therapy with minimal effects on normal renal cells.

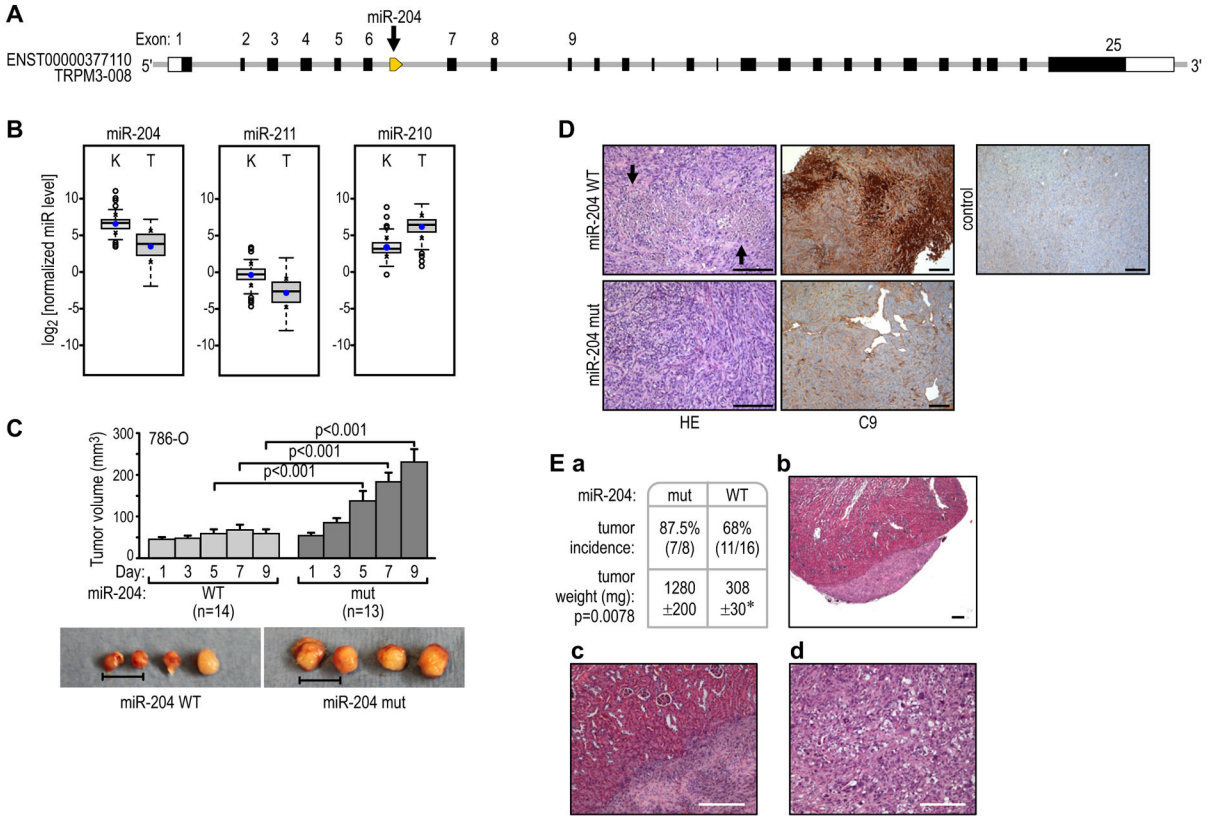

Figure 1. MiR-204 has tumor-suppressing activity in renal clear cell carcinoma

(A) Localization of miR-204 at the 5′ end of intron 6 of the host gene, *TRPM3*.

(B) Expression of miR-204, its paralog miR-211, and miR-210 in human ccRCC as compared with normal kidney tissue. Quantification of the indicated normalized miR levels (log_2) of the total unpaired kidney (K; n=114) and tumor (T; n=128) samples are shown. The boxes represent lower and upper quartiles separated by the median (thick horizontal line) and the whiskers extend up to the minimum and maximum values, excluding points that are outside the 1.5 interquartile range from the box (marked as circles). Means ± SD of each distribution are indicated by closed dots and crosses on the whiskers, respectively. All differences were statistically significant at $p<0.001$.

(C) Growth of pre-formed 786-O VHL(−) tumors in subcutaneous xenografts injected every other day over a period of 9 days with lentiviral particles of wild-type pre-miR-204 (WT) or pre-miR-204 with the 3-base-pair mutation (mut). The data are cumulative over two independent series of injections. Representative samples from each group of tumors are shown below. Scale bar = 1 cm.

(D) Representative images of H&E-stained or C9 antibody-probed sections from tumors injected with wild-type (top) or mutant (bottom) pre-miR-204. A section from a non-injected tumor stained for C9 is shown as a control. Scale bars = 200 μm.

(E) Incidence and size of RCC tumors resulting from transduced cells injected under the kidney capsules of nude mice (a). Example of H&E-stained sections of tumors formed by cells transduced with wild-type pre-miR-204 (b and c) or with mutant pre-miR-204 (d). Scale bar = 200 μm. See also Figure S1.

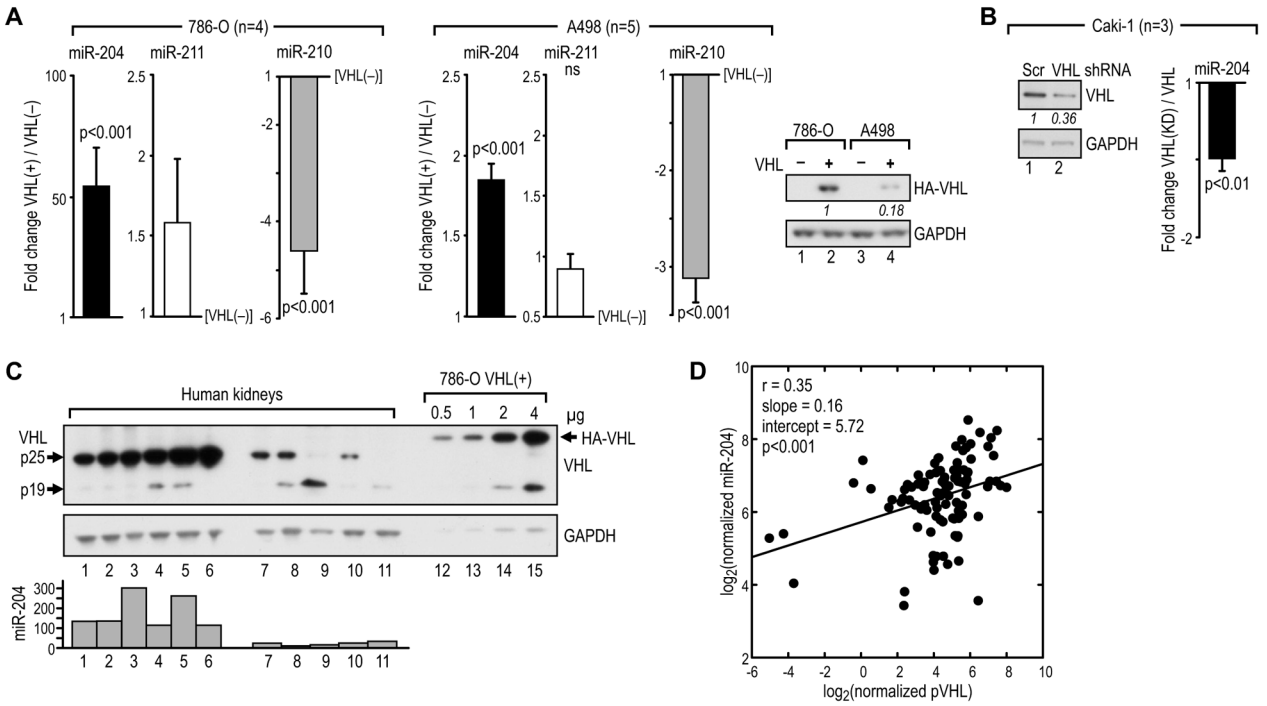

Figure 2. VHL positively regulates expression of miR-204

(A) Change in the level of miR-204, -211, and -210 in 786-O and A498 cells with reconstituted wild-type VHL as compared with the level of these miRs in VHL(−) cells. Reconstitution of human VHL (HA-VHL) is shown in a western blot.

(B) Change in miR-204 in Caki-1 with VHL knockdown as compared with cells transduced with scramble control shRNA. The western blot demonstrates knockdown of the endogenous VHL.

(C) Western blot of protein extracts form 6 human kidneys with high (lanes1-6) and low (lanes 7–11) levels of endogenous VHL. The indicated amounts of protein in extracts from 786-O cells with reconstituted VHL were blotted for comparison. Values for the normalized levels of miR-204 in each kidney are shown in a graph under the blot.

(D) Regression analysis of normalized miR-204 levels as a function of normalized VHL levels in kidneys (n=99). Data are $\log_2$-transformed. Each dot represents a sample and the solid line represents the linear regression fit, with the Pearson correlation coefficient (r) as well as the slope and intercept of the fitted line shown in the upper left corner of the box. See also Figure S2.

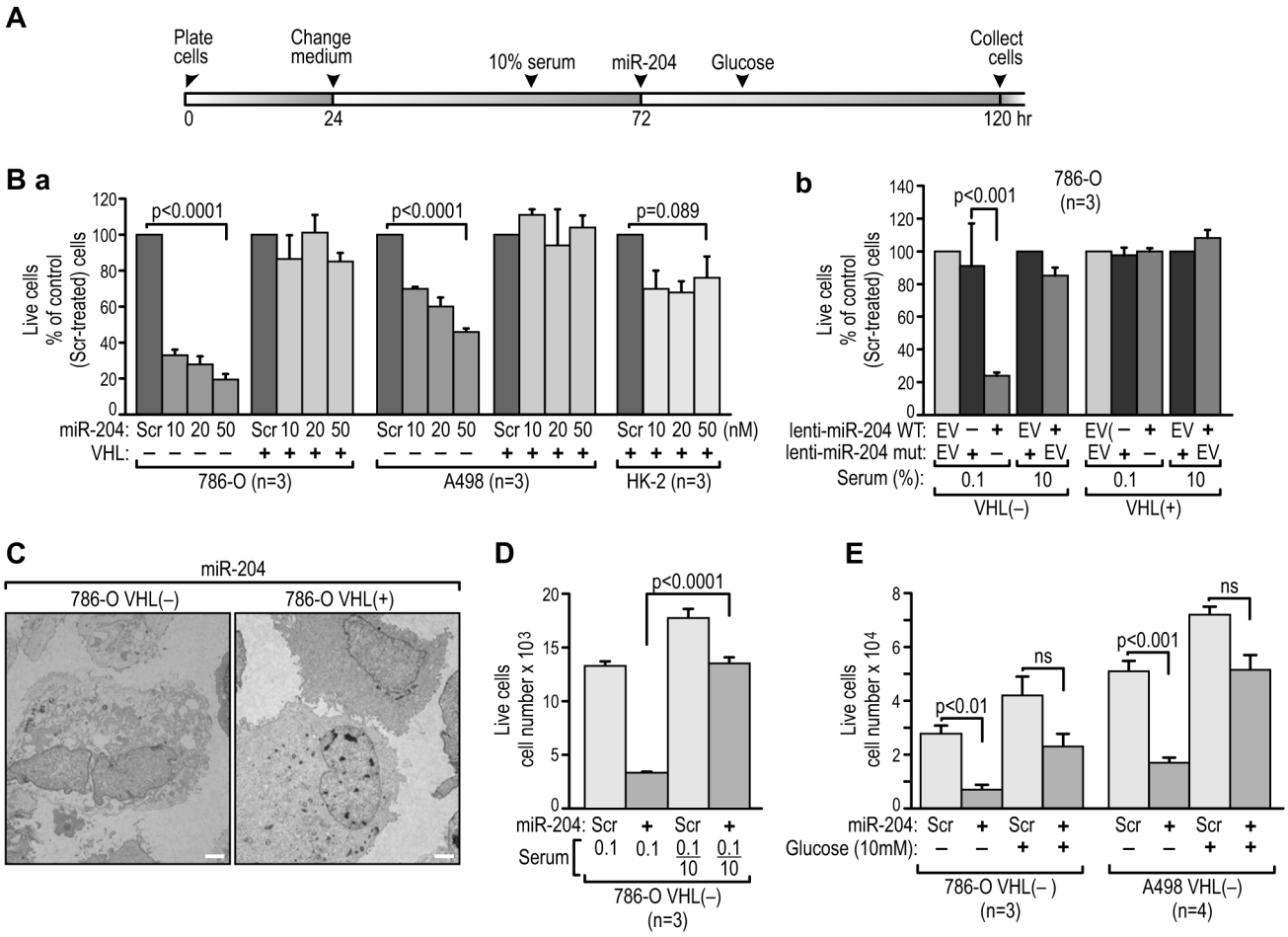

Figure 3. Cytotoxic effects of miR-204 in VHL(−) RCC cells are eliminated by reconstituted wild-type VHL

(A) Time line of the procedures performed during the course of experiments shown in B–E. In all experiments cells were plated at a density of 3,000 per well and the number of live cells treated with the scramble controls was between 10,000 and 20,000 at the time of collection (also see Figure 3C). Treatments were repeated at least three times in triplicate.

(B) Percentages of live cells determined by trypan blue exclusion 48 hr after administration of (a) short pre-miR-204 at the indicated concentrations as compared with the same cells treated with scramble control (Scr) at the same concentrations or (b) lentiviral miR-204 particles administered to the indicated cells as compared with the same cells treated with mutated miR-204 or empty virus (EV) in the presence of 0.1% or 10% serum. In (a) all experiments were performed in the presence of 0.1% serum.

(C) Example of a TEM microphotograph of VHL(-) cells dying from miR-204 cytotoxicity (left) and of live VHL(+) cells (right) under the same conditions. Scale bars = 2μm.

(D) Numbers of live cells when fresh medium containing 10% serum was given 6 hr before administration of miR-204 (see panel A).

(E) Numbers of live cells when medium was supplemented with 10 mM glucose after treatment with miR-204 (see panel A). See also Figure S3.

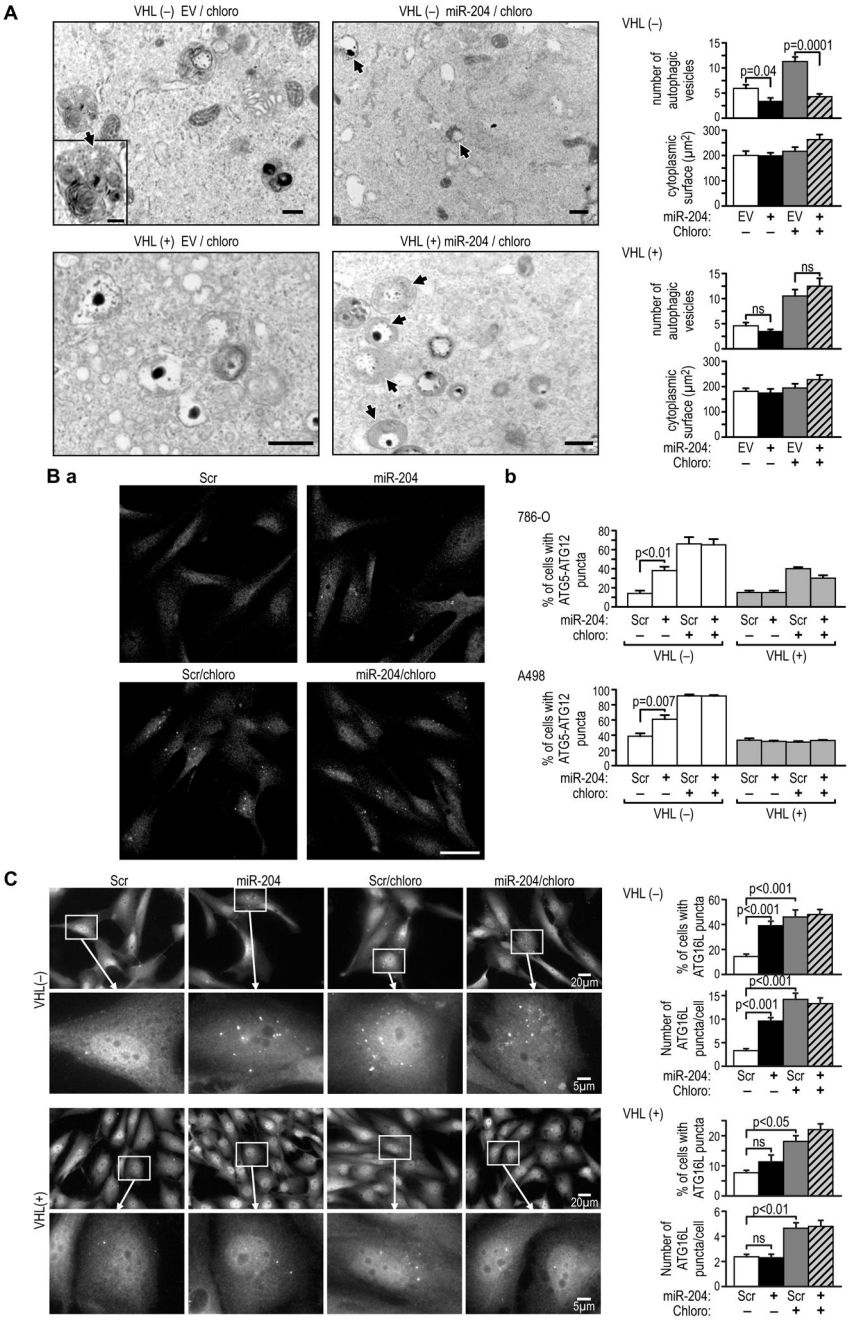

Figure 4. MiR-204 inhibits macroautophagy in VHL(−) cells, but not VHL(+) cells

(A) TEM microphotographs with quantification of the number of autophagic vesicles (AV) (top) and the cytoplasmic area (bottom) in 20 cells under the indicated conditions in 786-O VHL(−) and VHL(+) cells. Controls were treated with the same empty lentiviral constructs (EV). The arrows indicate AV. Scale bars = 1μm.

(B) Representative image of immunofluorescence staining for the endogenous ATG5-ATG12 complex in the indicated conditions in VHL(−) 786-O cells (a). (b) Quantification of the percent of cells with puncta vs. total number of cells in five independent fields containing on average 50 to 150 cells per field in each condition in 786-O and A498 cells. Controls were transfected with scramble construct. Scale bar = 50 μm.

(C) Representative image of immunofluorescence staining for endogenous ATG16L puncta in 786-O VHL(−) and VHL(+) cells under the indicated conditions. Percent of cells expressing puncta under the indicated conditions was calculated as in (B). 100 cells expressing puncta were analyzed for each condition, with the exception of non-treated controls where the number of cells with puncta was small and only 30 to 50 cells were counted. Control cells were treated with scramble construct. Scale bars are as indicated in the figure. All measurements shown in this figure were performed on cells grown in 0.1% serum and 24–30 hr after treatment with miR-204. This was approximately 24 hr before cell death was observed as shown in Figure 3B. See also Figure S4.

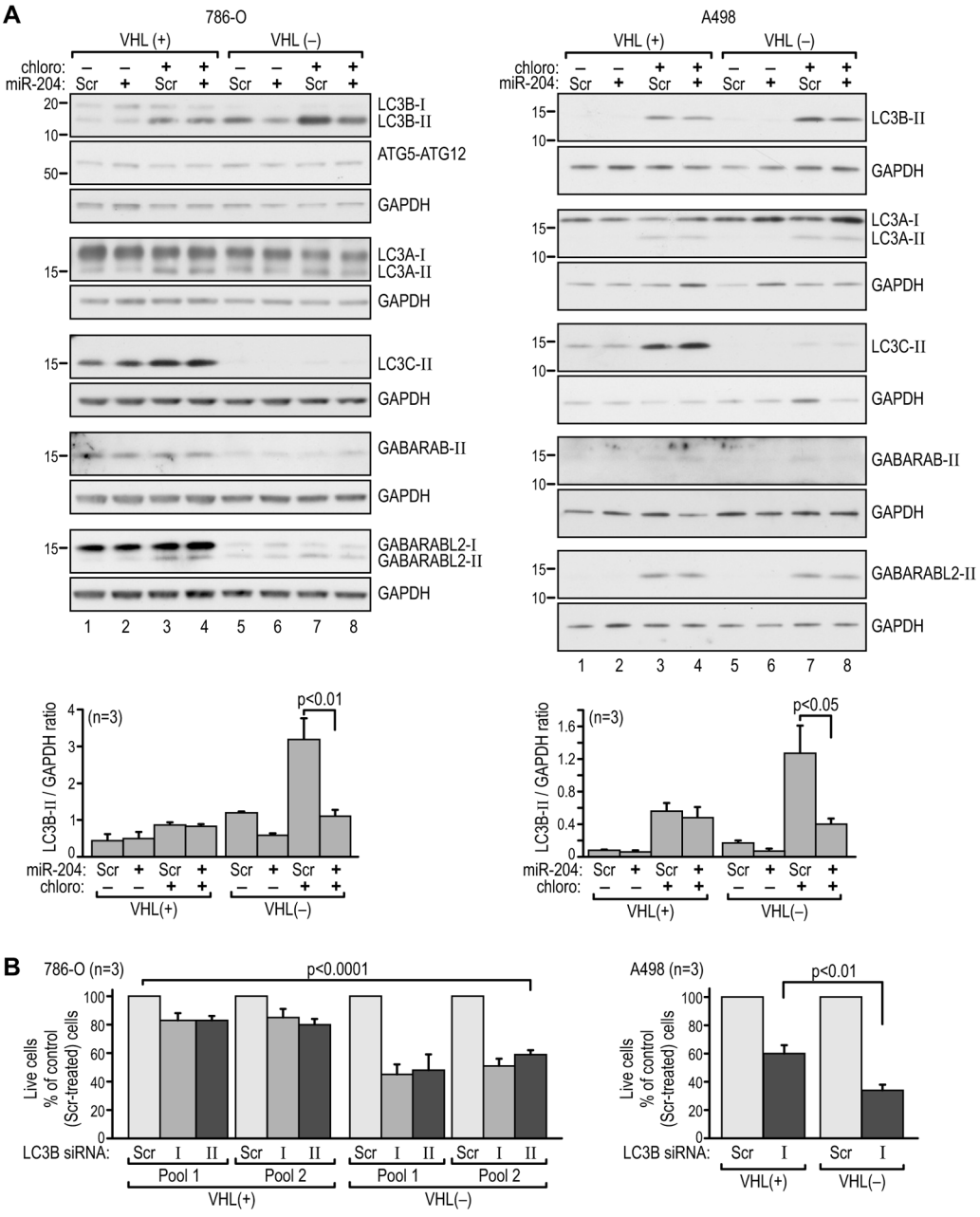

Figure 5. MiR-204 specifically represses accumulation of LC3B-II in the flux experiment

(A) Western blot analysis of LC3 orthologs in extracts from 786-O and A498 cells grown in 0.1% serum conditions. The experiment follows the same treatment sequence as shown in Figure 3A, with 100 μM chloroquine applied 24 hr after treatment with short pre-miR-204 or scramble control. The cells were collected after 1.5 hr in the case of 786-O cells and after 3 hr in the case of A498 cells, when saturating effects of chloroquine were observed based on the time-course experiments. This was approximately 24 hr before cell death was observed as shown in Figure 3B. Quantification of 3 independent experiments is shown at the bottom.

(B) Percentage of live cells measured using trypan blue analysis in 786-O and A498 VHL(+) and VHL(−) cells transfected with LC3B siRNA, where 100% corresponds to live cells

counted after transfection with scramble control construct. Time line as shown in Fig. S4A. See also Figure S5.

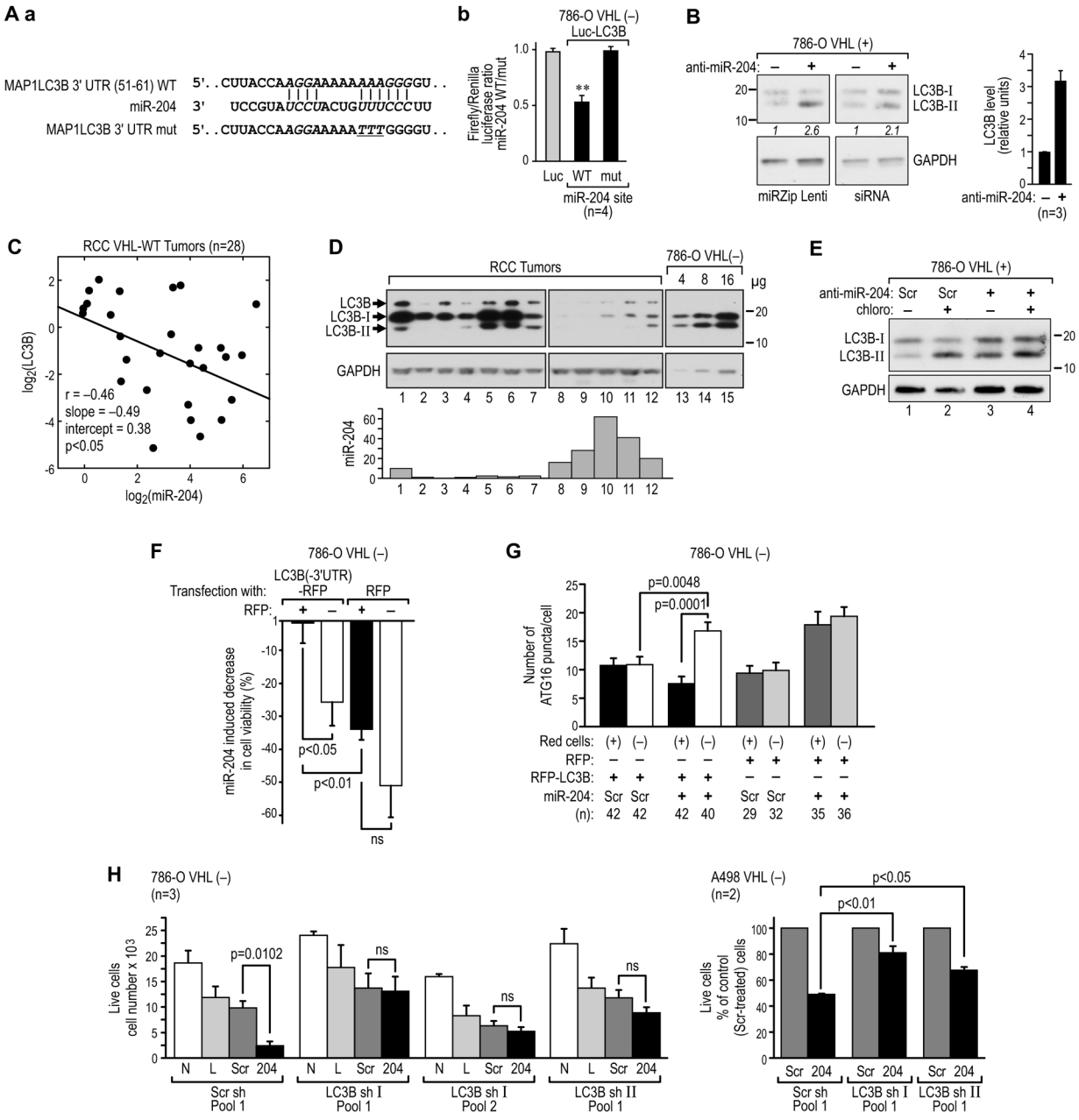

Figure 6. MAP1LC3B is a direct target of miR-204

(A) Sequence of the wild-type (WT) miR-204 site in the 3'UTR of LC3B, and mutation (mut) of the core binding site (a). (b) The 3'UTR of LC3B with the wild-type but not mutant miR-204 site confers regulation by miR-204 to the luciferase reporter construct.

(B) Effects of an anti–miR-204 lentiviral Zip or siRNAs on LC3B protein expression in 786-O VHL(+) RCC cells shown by western blot and quantification of 3 independent experiments.

(C) Regression analysis showing negative correlation between normalized miR-204 level and normalized LC3B protein level in human ccRCC tumors with the wild-type *VHL*, performed as described in Figure 2D.

(D) Representative western blot showing tumors with high and low levels of LC3B. Normalized values of miR-204 levels for each tumor are shown in a graph below the blot. Expression of LC3B in 786-O cells is shown as reference.
(E) Western blot showing accumulation of LC3B-II in 786-O VHL(+) cells treated with anti-miR-204 in the absence or presence of 100 μM chloroquine.
(F) 786-O VHL(−) cells transfected with RFP-LC3B or RFP were sorted, plated, and maintained for 48 hr in medium containing 0.1% serum. Cells were then treated with 25 nM short pre-miR-204 or scramble control construct and, 48 hr later, stained by DAPI. Fraction of live cells was determined among the stained and unstained cells in both conditions.
(G) Quantification of endogenous ATG16L puncta per cell in 786-O VHL(−) cells transfected with LC3B-RFP or RFP alone and treated with miR-204 as in (F). Red cells: (+) indicates cells expressing RFP fluorescence from either construct; (−) indicates cells that did not express RFP fluorescence. Numbers of cells (n) in which puncta were counted is shown below the graph.
(H) Effect of LC3B knockdown on cell death induced by miR-204. 786-O or A498 VHL(−) cells stably transfected with two different LC3B shRNAs or scramble construct were additionally transfected with miR-204 or scramble control. Two independent pools of 786-O cells expressing LC3B sh I RNA were used (Pool 1 and Pool 2). N, non-treated cells; L, cells transfected with Lipofectamine only; Scr, cells transfected with scramble pre-miR-204 control; 204, cells transfected with 50 nM of pre-miR-204. See also Figure S6.

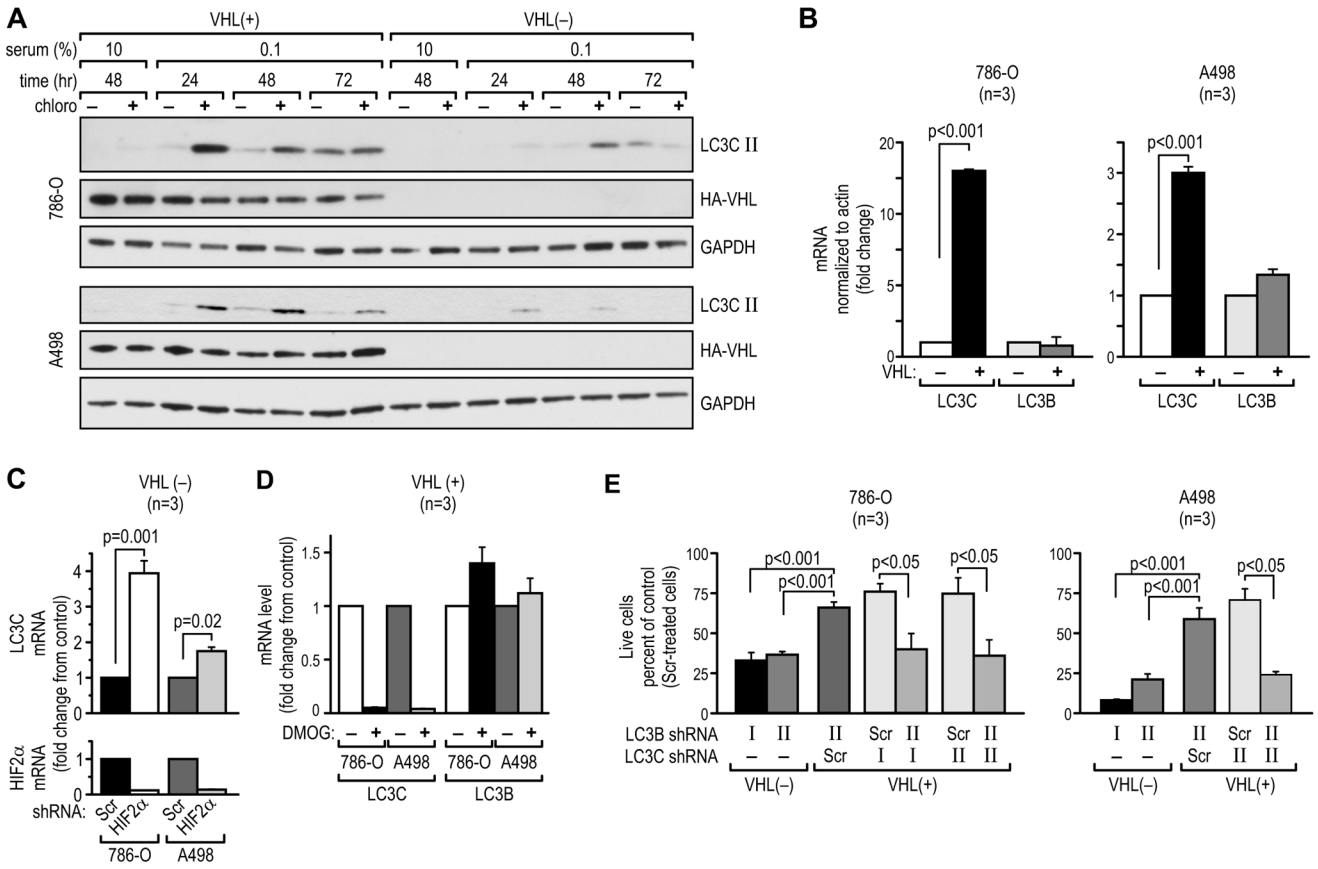

Figure 7. VHL-induced expression of LC3C protects RCC cells from inhibition of LC3B-dependent autophagy

(A) Western blot showing time course of LC3C-II induction in VHL(+) and VHL(−) 786-O and A498 cells in response to serum starvation.

(B) Quantitative RT-PCR for LC3C and LC3B mRNAs (48 hr of starvation) in VHL(+) as compared with VHL(−) cells.

(C) Quantitative RT-PCR for LC3C mRNA in VHL(−) cells where HIF-2α was knocked down by using siRNA.

(D) Quantitative RT-PCR for LC3C mRNA in VHL(+) cells where HIF was stimulated with DMOG (1 mM) for 16 hr.

(E) Effect of single LC3C or LC3B knockdown or of double LC3C/LC3B knockdown on the viability of indicated cells, as compared with scramble-treated cells. The timeline followed was the same as that shown in Figure 3A. See also Figure S7.

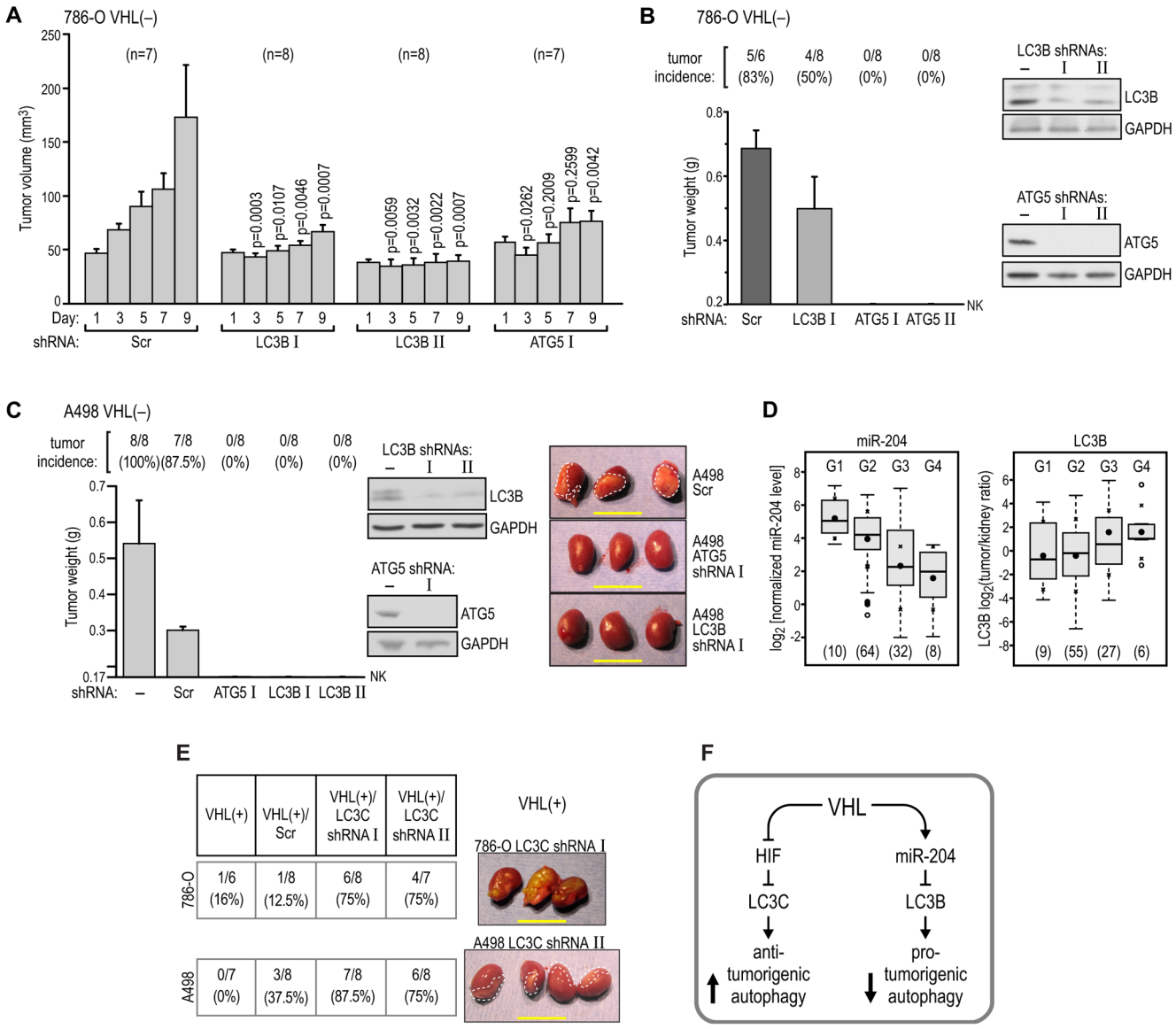

Figure 8. LC3B-dependent macroautophagy is necessary for RCC tumor growth

(A) Growth of tumors formed by 786-O VHL(−) cells in subcutaneous xenografts injected with packaged lentiviruses containing two different shRNAs against LC3B, or one against ATG5, as compared with the growth of control tumors injected with scramble sequence-containing virus. The number of mice in each experiment is shown in parentheses above the graph.

(B) Growth of tumors formed by pools of 786-O VHL(−) cells stably transfected with two different shRNAs against ATG5 or one against LC3B, and injected under the kidney capsule in nude mice. Western blots show levels of protein knockdown in stable pools of cells under conditions of 10% serum starvation. Cells were plated and grown for 48 hr in medium containing 10% serum before injection.

(C) Growth of tumors formed by pools of A498 VHL(−) cells stably transfected with two different shRNAs against LC3B and one against ATG5 and injected under the kidney capsule in nude mice. Western blots show levels of protein knockdown in stable pools of

cells. Cells were treated as in panel B. Photographs of representative tumors are shown with dashed lines drawn to help visualize the tumors.

(D) There is a significant decrease in the level of miR-204 ($p<0.001$) and a significant increase in the level of LC3B ($p<0.05$) correlating with tumor grade in human ccRCC tumors. Because of the small number of tumors classified as Grades 1 and 4, the statistical comparison was made between combined subpopulations of G1+G2 vs. G3+G4 tumors. The number of tumors of each grade is provided in parentheses at the bottom. Statistics were calculated as in Figure 1B. Means ± SD are shown.

(E) Formation of tumors in orthotopic xenografts by VHL(+) 786-O and A498 with stable knockdowns of LC3C using two different LC3C shRNAs in each cell line. The table lists numbers of mice analyzed and photographs of representative tumors are shown. Dashed lines help visualize tumorigenic infiltrate of A498 cells. All scale bars = 1 cm.

(F) Schematic representation of the role of VHL in the regulation of autophagy in RCC tumor growth. See also Figure S8.